Ultrastrong and Stiff Layered Polymer Nanocomposites

Paul Podsiadlo, *et al.*

Science **318**, 80 (2007);

DOI: 10.1126/science.1143176

The following resources related to this article are available online at www.sciencemag.org (this information is current as of October 5, 2007):

Updated information and services, including high-resolution figures, can be found in the online version of this article at:
http://www.sciencemag.org/cgi/content/full/318/5847/80

Supporting Online Material can be found at:
http://www.sciencemag.org/cgi/content/full/318/5847/80/DC1

This article **cites 31 articles**, 3 of which can be accessed for free:
http://www.sciencemag.org/cgi/content/full/318/5847/80#otherarticles

This article appears in the following **subject collections**:
Materials Science
http://www.sciencemag.org/cgi/collection/mat_sci

Information about obtaining **reprints** of this article or about obtaining **permission to reproduce this article** in whole or in part can be found at:
http://www.sciencemag.org/about/permissions.dtl

Science (print ISSN 0036-8075; online ISSN 1095-9203) is published weekly, except the last week in December, by the American Association for the Advancement of Science, 1200 New York Avenue NW, Washington, DC 20005. Copyright 2007 by the American Association for the Advancement of Science; all rights reserved. The title *Science* is a registered trademark of AAAS.

References and Notes

1. J. A. Rogers, Z. Bao, H. E. Katz, A. Dodabalapur, in *Thin-Film Transistors*, C. R. Kagan, P. Andry, Eds. (Marcel Dekker, New York, 2003), pp. 377–425.
2. R. Brown, A. Pomp, C. M. Hart, D. M. de Leeuw, *Science* **270**, 972 (1995).
3. V. C. Sundar *et al.*, *Science* **303**, 1644 (2004).
4. L.-L. Chua *et al.*, *Nature* **434**, 194 (2005).
5. M. J. Panzer, C. D. Frisbie, *J. Am. Chem. Soc.* **127**, 6960 (2005).
6. A. Facchetti, M.-H. Yoon, T. J. Marks, *Adv. Mater.* **17**, 1705 (2005).
7. A. Salleo, M. L. Chabinyc, M. S. Yang, R. A. Street, *Appl. Phys. Lett.* **81**, 4383 (2002).
8. T. Takahashi, T. Takenobu, J. Takeya, Y. Iwasa, *Appl. Phys. Lett.* **88**, 033505 (2006).
9. N. Stutzmann, R. H. Friend, H. Sirringhaus, *Science* **299**, 1881 (2003).
10. M.-H. Yoon, C. Kim, A. Facchetti, T. J. Marks, *J. Am. Chem. Soc.* **128**, 12851 (2006).
11. L. Berthier *et al.*, *Science* **310**, 1797 (2005).
12. L. A. Deschenes, D. A. Vanden Bout, *Science* **292**, 255 (2001).
13. P. G. Debenedetti, F. H. Stillinger, *Nature* **410**, 259 (2001).
14. J. A. Forrest, K. Dalnoki-Veress, J. R. Dutcher, *Phys. Rev. E Stat. Phys. Plasmas Fluids Relat. Interdiscip. Top.* **56**, 5705 (1997).
15. C. L. Jackson, G. B. McKenna, *J. Non-Cryst. Solids* **131-133**, 221 (1991).
16. S. Kawana, R. A. L. Jones, *Phys. Rev. E Stat. Phys. Nonlin. Soft Matter Phys.* **63**, 021501 (2001).
17. K. Fukao, Y. Miyamoto, *Phys. Rev. E Stat. Phys. Plasmas Fluids Relat. Interdiscip. Top.* **61**, 1743 (2000).
18. J. A. Forrest, K. Dalnoki-Veress, J. R. Stevens, J. R. Dutcher, *Phys. Rev. Lett.* **77**, 2002 (1996).
19. C. J. Ellison, M. K. Mundra, J. M. Torkelson, *Macromolecules* **38**, 1767 (2005).
20. J. A. Forrest, K. Dalnoki-Veress, *Adv. Coll. Interf. Sci.* **94**, 167 (2001).
21. O. Prucker *et al.*, *Macromol. Chem. Phys.* **199**, 1435 (1998).
22. These coefficients were estimated from the data provided by (*19*).
23. H. Klauk, U. Zschieschang, J. Pflaum, M. Halik, *Nature* **445**, 745 (2007).
24. R. Ruiz, A. Papadimitratos, A. C. Mayer, G. G. Malliaras, *Adv. Mater.* **17**, 1795 (2005).
25. C. D. Dimitrakopoulos *et al.*, *Science* **283**, 822 (1999).
26. A. L. Briseno *et al.*, *Nature* **444**, 913 (2006).
27. Materials and methods are available as supporting material on *Science* Online.
28. K. Puntambekar, J. Dong, G. Haugstad, C. D. Frisbie, *Adv. Funct. Mater.* **16**, 879 (2006).
29. K. N. N. Unni, S. Dabos-Seignon, J.-M. Nunzi, *J. Mater. Sci.* **41**, 317 (2006).
30. C. D. Dimitrakopoulos, A. R. Brown, A. Pomp, *J. Appl. Phys.* **80**, 2501 (1996).
31. H. Yanagisawa, T. Tamaki, M. Nakamura, K. Kudo, *Thin Solid Films* **464-465**, 398 (2004).
32. D. L. Smith, *Thin-Film Deposition: Principles and Practice* (McGraw Hill, New York, 1995).
33. Z. Zhang, M. G. Lagally, *Science* **276**, 377 (1997).
34. K. Tanaka, A. Takahara, T. Kajiyama, *Macromolecules* **33**, 7588 (2000).
35. S. Ge *et al.*, *Phys. Rev. Lett.* **85**, 2340 (2000).
36. S. Steudel *et al.*, *Appl. Phys. Lett.* **85**, 4400 (2004).
37. D. Knipp, R. A. Street, A. R. Volkel, A. Ho, *J. Appl. Phys.* **93**, 347 (2003).
38. S. Guruvenket, G. M. Rao, M. Komath, A. M. Raichur, *Appl. Surf. Sci.* **236**, 278 (2004).
39. R. W. Paynter, *Surf. Interface Anal.* **33**, 862 (2002).
40. We thank J. M. Torkelson and J. Kim for helpful discussion. This work was supported by the Air Force Office of Scientific Research (grant STTRFA 9550-04-0080), Polyera Corp., and the NSF Materials Research Science and Engineering Centers program through the Northwestern Materials Research Center (grant DMR-0520513). This contribution is dedicated to Prof. G. A. Pagani on the occasion of his 70th birthday.

Supporting Online Material
www.sciencemag.org/cgi/content/full/318/5847/76/DC1
Materials and Methods
Figs. S1 to S4
Table S1
Reference

13 June 2007; accepted 7 September 2007
10.1126/science.1146458

Ultrastrong and Stiff Layered Polymer Nanocomposites

Paul Podsiadlo,[1] Amit K. Kaushik,[2] Ellen M. Arruda,[2,3] Anthony M. Waas,[2,4] Bong Sup Shim,[1] Jiadi Xu,[5] Himabindu Nandivada,[1] Benjamin G. Pumplin,[2] Joerg Lahann,[1,3,6] Ayyalusamy Ramamoorthy,[5] Nicholas A. Kotov[1,6,7]*

Nanoscale building blocks are individually exceptionally strong because they are close to ideal, defect-free materials. It is, however, difficult to retain the ideal properties in macroscale composites. Bottom-up assembly of a clay/polymer nanocomposite allowed for the preparation of a homogeneous, optically transparent material with planar orientation of the alumosilicate nanosheets. The stiffness and tensile strength of these multilayer composites are one order of magnitude greater than those of analogous nanocomposites at a processing temperature that is much lower than those of ceramic or polymer materials with similar characteristics. A high level of ordering of the nanoscale building blocks, combined with dense covalent and hydrogen bonding and stiffening of the polymer chains, leads to highly effective load transfer between nanosheets and the polymer.

A critical challenge in nanocomposite fabrication is the ability to realize materials that allow the transfer of the exceptional mechanical properties (i.e., tensile strength, σ_{UTS}, and Young's modulus, E) of the nanoscale materials to the macroscale properties of the bulk materials. Nanoparticle-filled polymer composites based on these structural elements have mechanical properties that fall far below the expected theoretical and experimentally determined values of the individual building blocks, except at low volume fractions of the reinforcement (*1*–*9*). The deficiency in the properties of the composite is largely related to the difficulty of obtaining well-dispersed large volume fractions of the reinforcing nanomaterials and a lack of structural control. The difficulty is also associated with realizing an effective load transfer from the polymeric matrix to the nanoscale components and the insufficiently understood mechanical interactions of the two constituents at the nanoscale. We demonstrate that it is possible to produce composites with properties that approach the theoretical maxima using spatial and orientational control of clay platelets in a polymer matrix at the nanoscale and retaining this order at the macroscale.

Hybrid organic-inorganic nanocomposites of polymer and clay nanoplatelets have received special attention because of the very low cost of the inorganic component, relatively simple preparation, and fairly predictable stiffening behavior when introduced into polymers (*9*, *10*). Montmorillonite (MTM) clay (~1–nm–thick-by-100– to 1000–nm–diameter sheets) has been extensively used for this purpose because it is readily available and has exceptional mechanical properties. The in-plane modulus of elasticity has been estimated by Monte Carlo simulations to be ~270 GPa (*6*). Although composites incorporating 50 volume % of MTM should theoretically have stiffness values on the order of 100 GPa, values achieved to date with MTM platelets are at least one order of magnitude lower. This is because, in general, less than ~10 weight % (wt %) of the clay can be incorporated homogeneously as completely dispersed silicates rather than intercalated structures into the polymer because of the strong tendency of the clay to aggregate and phase separate. Further increases in the volume of the clay content have either marginally increased or even reduced both the strength and stiffness (*9*, *11*).

We approached preparation of the clay nanocomposite by using a bottom-up assembly process called layer-by-layer (LBL) assembly (*12*). The LBL process is based on sequential adsorption of nanometer-thick monolayers of oppositely charged compounds (such as polyelectrolytes, charged nanoparticles, and biological macromolecules) to form a multilayered structure with nanometer-level control over the architecture. In the past, we have used the LBL technique to prepare nanocomposites from carbon nanotubes (CNTs) that have $\sigma_{\mathrm{UTS}} \sim 220$ MPa (*13*, *14*). We have also shown that the organization of LBL composites has many analogies with the structure

---

[1] Department of Chemical Engineering, University of Michigan, Ann Arbor, MI 48109–2136, USA. [2] Department of Mechanical Engineering, University of Michigan, Ann Arbor, MI 48109–2125, USA. [3] Program in Macromolecular Science and Engineering, University of Michigan, Ann Arbor, MI 48109–2140, USA. [4] Department of Aerospace Engineering, University of Michigan, Ann Arbor, MI 48109–2140, USA. [5] Biophysics Research Division and Department of Chemistry, University of Michigan, Ann Arbor, MI 48109–1055, USA. [6] Department of Biomedical Engineering, University of Michigan, Ann Arbor, MI 48109–2099, USA. [7] Department of Materials Science and Engineering, University of Michigan, Ann Arbor, MI 48109–2136, USA.

*To whom correspondence should be addressed. E-mail: kotov@umich.edu

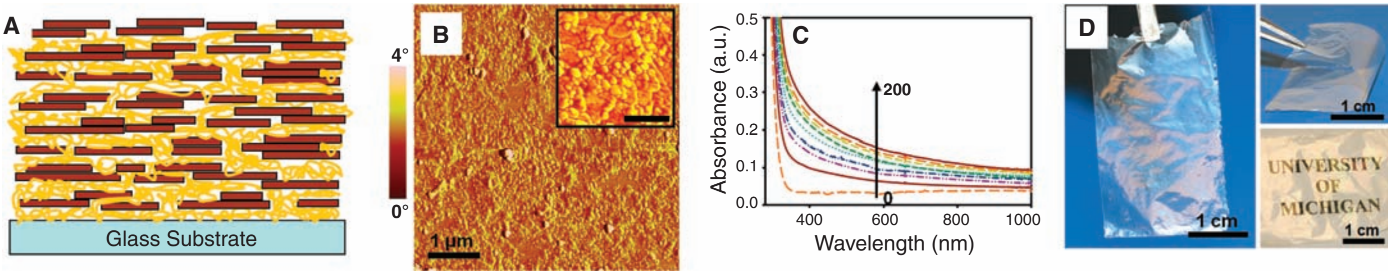

Fig. 1. Preparation of PVA/MTM nanocomposites. (**A**) Schematic representation of the internal architecture of the PVA/MTM nanocomposite (picture shows 8 bilayers). (**B**) ATM phase image of a single PVA/MTM bilayer adsorbed on top of a silicon wafer. (Inset) Close up of the main image showing individual MTM platelets more clearly. Scale bar in inset, 400 nm. (**C**) Compilation of UV/VIS absorbance spectra collected after multiples of 25 bilayers of PVA/MTM composite deposited on both sides of a microscope glass slide up to 200 bilayers. a.u., arbitrary units. (**D**) Free-standing, 300-bilayer PVA/MTM composite film showing high flexibility and transparency. The lower image was taken at an angle to show diffraction colors.

Fig. 2. Scanning electron microscopy characterization of a 300-bilayer, free-standing PVA/MTM nanocomposite. (**A**) Cross section of the film. Arrows indicate the span of the cross section. (**B**) Close-up of the cross section showing the separation of layers. (**C**) Top-down view of a fracture edge of the composite after tensile testing. Dashed line indicates edge of the sample. (**D**) Top-down view of the composite's surface. The slight separation of the layers seen in (A) and (B) is due to a shearing force resulting from cutting the sample with a razor blade during scanning electron microscopy sample preparation.

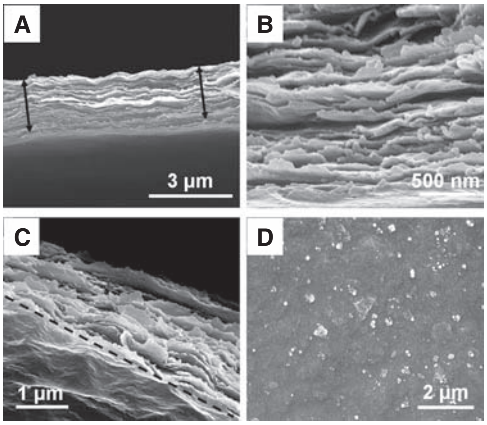

of one of the toughest natural mineral-based materials, nacre (*15*). In this respect, LBL assembly of negatively charged nanosheets of hectorite or MTM clays with a poly(diallyldimethylammonium chloride) (PDDA) polycation led to the formation of a material with σ_{UTS} ~100 MPa and a tangent stiffness after strain stiffening of ~11 GPa (*15*, *16*). Although fairly high, these values are still below the theoretical limits for these materials, based on the mechanical properties of individual nanotubes and/or clay sheets.

A traditional LBL process of sequentially coating a surface with nanometer-thick layers of poly(vinyl alcohol) (PVA) and MTM by immersing a glass substrate in dilute solutions of the components was used in this study (*17*–*19*). Ellipsometry and ultraviolet/visible (UV/VIS) spectroscopy (Fig. 1 and fig. S1) revealed linear and uniform growth.

Characterization of the assembly with the use of atomic force microscopy (AFM) (Fig. 1) and scanning electron microscopy (Fig. 2) verified dense coverage of the nanoplatelets and their strictly planar orientation. The electron microscopy characterization provided thickness measurements of 1.0 ± 0.1 µm (SEM) and 1.5 ± 0.1 µm (SEM) for 200- and 300-bilayer films, respectively, indicating an average of ~5 nm of thickness per bilayer (Fig. 2A). Nearly identical thickness was obtained from ellipsometry for a 300-bilayer film grown on a silicon wafer: 1.480 ± 0.004 µm (SEM). The cross section also revealed a well-defined layered architecture.

We note that PVA is uncharged, unlike many other polymeric materials used in LBL. Nevertheless, it produces a stronger composite than do other polymers that undergo electrostatic attraction to the clay sheets (*19*–*21*). The PVA/MTM pair has two unique properties. The first is the high efficiency of hydrogen bonding. Atomic modeling revealed that the geometry of SiO_4 tetrahedrons on the surface of the alumosilicates is conducive to cooperative hydrogen bonding (the Velcro effect). The distances between the O atoms of clay and H atoms of PVA are 2.75 and 2.65 Å, respectively, which makes hydrogen bonding epitaxial (fig. S3). Second, a substantial part of the efficient load transfer between the polymer and the inorganic building block is attributed to the cyclic cross-linking to Al substitution present on the surface of MTM sheets and to Al atoms located along the edges of the MTM platelets (*22*). These Al atoms are easily accessible (Fig. 3A) to the macromolecules, unlike similar groups in the middle of the sheets. An atom of Al, two atoms of O, and three atoms of C from PVA participating in this bond form a six-membered ring structure, which is known to be particularly stable (Fig. 3A). Experimental data from Fourier transform infrared (FTIR) spectroscopy, nuclear magnetic resonance (NMR), and x-ray photoelectron scattering (XPS) spectroscopy, point to the formation of the Al–PVA covalent linkages. As such, we see a characteristic shift in the XPS spectra of Al from 74.4 to 74.9 eV (1 and 2 in Fig. 3B); concomitantly, a change in the ratio of carbon XPS peaks at 284.8 eV ($-C-H_2$) and 286.2 eV ($-C-O-H$) was observed (Fig. 3C). The formation of Al–PVA bonds can be further confirmed by the appearance of the characteristic FTIR vibration of Al–O–C (Fig. 3D, inset) at 848 cm^{-1} (*22*) and the strong suppression of the C–O–H band at 3290 cm^{-1} (Fig. 3E), which correlate well with the condensation of hydroxyls at Al sites with those from PVA groups. The NMR spectra of ^{27}Al (fig. S4) remain the same as expected because the coordination environment of Al (octahedral) did not change. The nanometer-scale organization and the layered structure of the composite provide the necessary conditions for the formation of multiples of such cyclic linkages.

Films were treated with glutaraldehyde (GA) after LBL assembly to further the bonding and load transfer between the –OH groups and the clay surface. GA is a highly efficient cross-linking agent for PVA (*23*, *24*) that forms covalent acetal bridges between –OH groups of the polymer chains (fig. S5), as well as the hydroxyl groups present on the MTM sheets and particularly on their edges. Solid-state NMR techniques revealed dramatic changes in the spectra before and after GA treatment (fig. S4). We can also see clear evidence of a reaction between GA and clay from NMR (fig. S5) and FTIR spectra (fig. S6), which indicates that this type of cross-linking further increases connectivity between PVA and clay sheets as well as the clay particles themselves.

Cross-linked free-standing films showed high uniformity, strength, flexibility, and remarkable transparency (Fig. 1D). UV/VIS spectra of the 300-bilayer free-standing films showed 80 to 90% transparency across the visible light spectrum, whereas pure PVA showed 90 to 95% transparency (fig. S7). Thermogravimetric analysis showed that the same films were composed in ~70 wt % (~50 volume %) of the MTM (fig. S8). This can be explained by the nanoscale dimensions of the inorganic phase and the nearly perfect orientation and fine dispersion of the nanoplatelets. UV/VIS spectroscopy also showed Fabry-Perot patterns (*25*, *26*), which are a further indication of high uniformity in the film.

Evaluation of mechanical properties by microtensile tests yielded remarkable results even

Fig. 3. Characterization of PVA and MTM molecular interactions. (**A**) Energy-optimized geometry of bonding between PVA and MTM via Al substitution sites obtained by computer calculations with the AM1 semi-empirical algorithm. (Right) Enlarged portion of the six-membered cycle formed between PVA and MTM. Al, purple; O, red; H, light gray; Si, dark gray; C, green. (**B**) Al 2p orbital XPS spectra for (1) MTM, (2) PVA/MTM nanocomposite, and (3) PVA/MTM nanocomposite with GA cross-linking. A positive energy shift is indicative of the increased oxidation state of the Al. (**C**) C 1s orbital XPS spectra for (1) PVA, (2) PVA/MTM composite, and (3) PVA/MTM composite with GA cross-linking. XPS spectra were deconvoluted in component peaks corresponding to the different oxidation states of C. The major peaks at 284.8 and 286.2 eV correspond to $-C-H_2$ and $-C-O-H$ carbons, respectively. (**D**) Comparison of FTIR spectra for (1) PVA/MTM composite and (2) MTM. (Inset) Close-up of the major peaks. Arrow points to the characteristic vibration peak at 848 cm^{-1}. (**E**) Comparison of FTIR spectra for pure (1) PVA and (2) PVA/MTM composite. The spectrum of PVA/MTM shows suppression of the C–O–H vibrations because of covalent binding with the MTM surface.

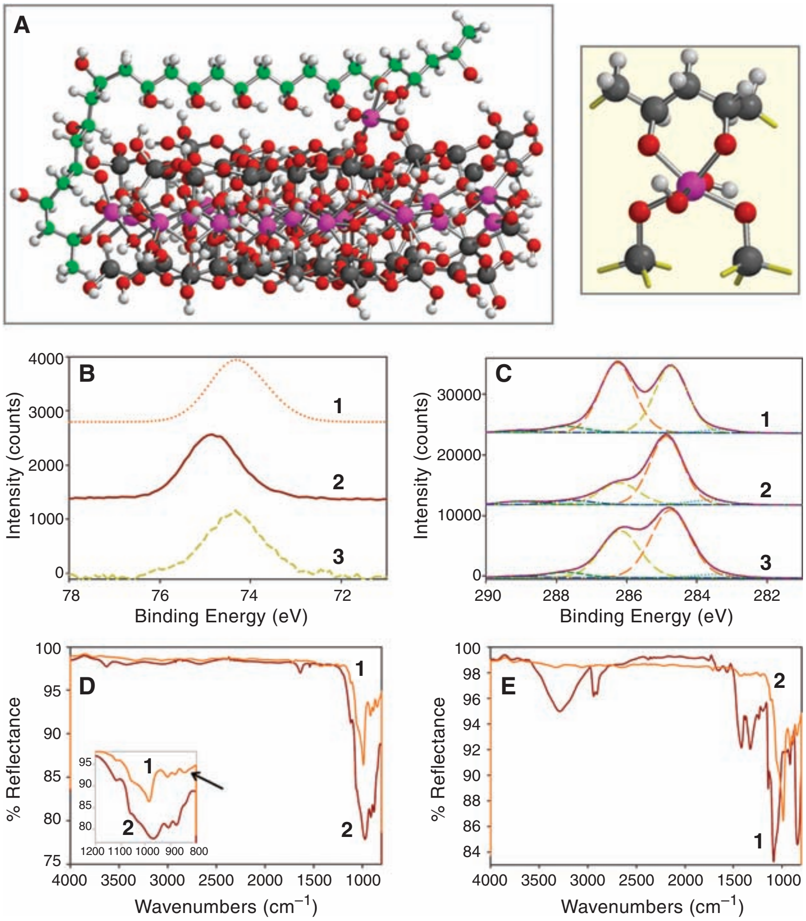

without GA cross-linking (Fig. 4, Table 1, and fig. S2). The nanocomposite displayed ~four times higher strength and nearly one order of magnitude higher modulus when compared with pure PVA polymer. GA cross-linking increased the strength, stiffness, and brittleness of both pure PVA and the PVA/MTM composite. (Fig. 4, A and B) The ultimate tensile strength increased by nearly a factor of 3 over the uncross-linked PVA/MTM strength and 10 times in comparison with that of pure PVA, to values as high as 480 MPa. The modulus of the PVA/MTM with GA exceeded that of uncross-linked PVA/MTM by one order of magnitude and that of pure PVA by two orders of magnitude, with the highest values reaching 125 GPa. The modulus of PVA/MTM with GA is comparable to that of various grades of Kevlar (*27*–*29*), *E* ~ 80 to 220 GPa, and exceeds the stiffness of the strongest CNT-based fibers (*30*). Additionally, unlike PDDA-MTM composites, the PVA/MTM films with GA cross-linking showed exceptional stability under humid conditions (fig. S9), which is consistent with the covalent character of the bonds responsible for load transfer.

Theoretical estimates for nanocomposite properties with nanometer-scale spacing of constituents in a polymer and such a large volume fraction of the filler are not available, and the currently recognized theories from the filled-rubber literature are not entirely applicable (*31*).

Fig. 4. Mechanical and thermal properties of PVA and PVA/MTM nanocomposites. (**A**) Stress-strain curves for 300-bilayer PVA/MTM composites (1) without and (2) with GA cross-linking. (**B**) Stress-strain curves for pure PVA polymer (1) without and (2) with GA cross-linking. The stress-strain curves were obtained from a home-built tensiometer (see supporting online material). (**C** to **F**) Differential scanning calorimetric analyses results for PVA polymer (C) without and (D) with GA cross-linking and for PVA/MTM (E) without and (F) with GA cross-linking. The DSC scans follow (1) heat, (2) cool, (3) heat cycles, as indicated by the numbering on the graphs.

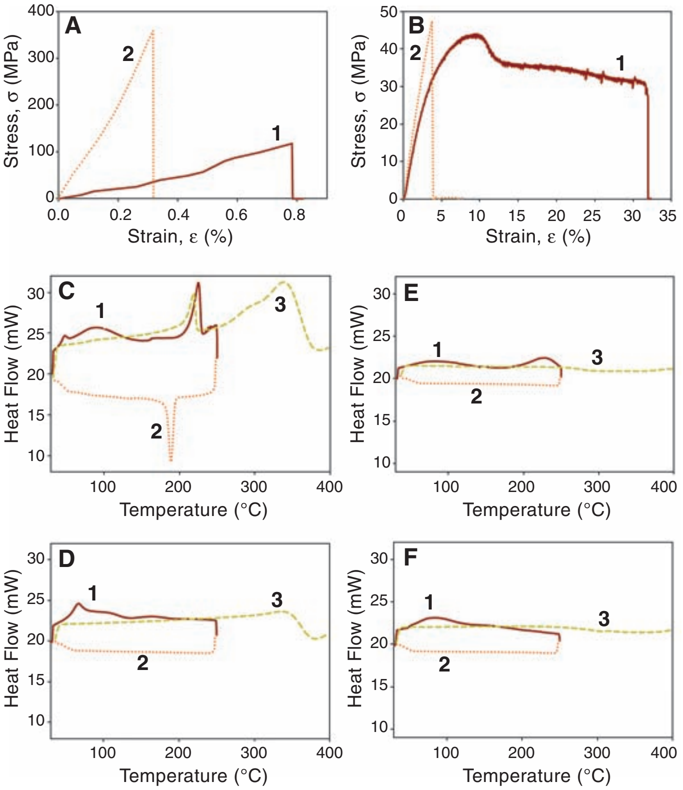

Table 1. Summary of mechanical properties for PVA and its nanocomposites. The data are mean ± SD. The tensile strengths reported were obtained using both a commercially available servohydraulic test system and a custom in-house–built tensiometer (fig. S2). The moduli were obtained using the custom-built tensiometer. *N* indicates the minimum number of experimental data points that we used in the statistical calculations.

Sample type (*N*)	Tensile strength σ_{UTS} (MPa)	Modulus E' (GPa)	Ultimate strain ε (%)
PVA (5)	40 ± 4	1.7 ± 0.2	35 ± 4
PVA with GA (5)	40 ± 10	2.0 ± 0.5	3.3 ± 1.3
PDDA (5)	12 ± 4	0.2 ± 0.03	48 ± 9
PDDA-MTM (*)	100 ± 10	11 ± 2	10 ± 2
PVA/MTM (5)	150 ± 40	13 ± 2	0.7 ± 0.2
PVA/MTM with GA (5)	400 ± 40	106 ± 11	0.33 ± 0.04

*Data are the previously published results by Tang *et al.* (*15*) for 1.2-to-4.9–μm–thick (50 to 200 bilayers) samples tested at relative humidity of 32%.

We believe that the explanation of these results lies in the effective stiffening of the PVA matrix (due to constrained motion of the polymer chains) because of its close proximity to and many interactions with the MTM platelets. The evidence of this reinforcement mechanism comes from differential scanning calorimetry (DSC) analysis (Fig. 3, C to F), which shows suppression of the thermal motion of the PVA when it is constrained between dispersed nanoplatelets. This effect should result in a shift in glass transition temperature (T_g) toward the higher values. However, the overall suppression of motion makes the actual T_g of the polymer not very well defined for such systems, as can be seen in the width of the corresponding DSC peaks. A similar effect can be seen from a comparison of polymer melting temperatures (T_m) between pure PVA (Fig. 4C) and PVA/MTM (Fig. 4E). Whereas the T_m in PVA is sharp and very well defined, PVA/MTM shows strong suppression and broadening of the peak. An additional consequence of such stiffening is that traditional theories of composite mechanics using the bulk properties of pure polymers are difficult to apply to composites with high contents of a uniformly distributed inorganic phase. Mechanical-property enhancement in the GA cross-linked PVA/MTM is a result of an increase in the likelihood that a polymer chain in the PVA/MTM with GA system interacts strongly with two or more clay platelets, thereby improving the particle-to-matrix-to-particle load-transfer process over that in the PVA/MTM system.

In conclusion, reinforcement in polymer-nanoplatelet systems such as PVA/MTM is the result of several mechanisms operating at the nanoscale. The degree of structural organization (afforded by the LBL process) of the clay platelets in the composite maximizes the number of polymer/MTM interactions and constrains the polymer-chain motion, which results in a highly efficient load transfer between the polymer phase and the stiff MTM platelets.

References and Notes

1. M. M. J. Treacy, T. W. Ebbesen, J. M. Gibson, *Nature* **381**, 678 (1996).
2. M.-F. Yu *et al.*, *Science* **287**, 637 (2000).
3. O. Breuer, U. Sundararaj, *Polym. Compos.* **25**, 630 (2004).
4. G. Van Lier, C. Van Alsenoy, V. Van Doren, P. Geerlings, *Chem. Phys. Lett.* **326**, 181 (2000).
5. A. Sturcova, G. R. Davies, S. J. Eichhorn, *Biomacromolecules* **6**, 1055 (2005).
6. O. L. Manevitch, G. C. Rutledge, *J. Phys. Chem. B* **108**, 1428 (2004).
7. J. J. Mack *et al.*, *Adv. Mater.* **17**, 77 (2005).
8. M. A. S. A. Samir, F. Alloin, A. Dufresne, *Biomacromolecules* **6**, 612 (2005).
9. S. S. Ray, M. Okamoto, *Prog. Polym. Sci.* **28**, 1539 (2003).
10. E. P. Giannelis, *Adv. Mater.* **8**, 29 (1996).
11. G. Lagaly, *Appl. Clay Sci.* **15**, 1 (1999).
12. G. Decher, *Science* **277**, 1232 (1997).
13. A. A. Mamedov *et al.*, *Nat. Mater.* **1**, 190 (2002).
14. M. Olek *et al.*, *Nano Lett.* **4**, 1889 (2004).
15. Z. Tang, N. A. Kotov, S. Magonov, B. Ozturk, *Nat. Mater.* **2**, 413 (2003).
16. E. R. Kleinfeld, G. S. Ferguson, *Science* **265**, 370 (1994).
17. P. T. Hammond, *Adv. Mater.* **16**, 1271 (2004).
18. C. Jiang, V. V. Tsukruk, *Adv. Mater.* **18**, 829 (2006).
19. Z. Tang, Y. Wang, P. Podsiadlo, N. A. Kotov, *Adv. Mater.* **18**, 3203 (2006).
20. P. Podsiadlo, Z. Tang, B. S. Shim, N. A. Kotov, *Nano Lett.* **7**, 1224 (2007).
21. P. Podsiadlo, Z. Liu, D. Paterson, P. B. Messersmith, N. A. Kotov, *Adv. Mater.* **19**, 949 (2007).
22. A. A. Bonapasta, F. Buda, P. Colombet, *Chem. Mater.* **12**, 738 (2000).
23. M. Nagy, E. Wolfram, T. Varadi, *Prog. Colloid Polym. Sci.* **60**, 138 (1976).
24. D. Braun, E. Walter, *Colloid Polym. Sci.* **258**, 795 (1980).
25. Y. Guan *et al.*, *J. Phys. Chem. B* **110**, 13484 (2006).
26. A. Mamedov, J. Ostrander, F. Aliev, N. A. Kotov, *Langmuir* **16**, 3941 (2000).
27. M. Cheng, W. Chen, T. Weerasooriya, *J. Eng. Mater. Technol.* **127**, 197 (2005).
28. C. Y. Yue, G. X. Sui, H. C. Looi, *Compos. Sci. Technol.* **60**, 421 (2000).
29. A. M. Hindeleh, S. Abdo, *Polym. Commun.* **30**, 184 (1989).
30. A. B. Dalton *et al.*, *Nature* **423**, 703 (2003).
31. J. S. Bergstrom, M. C. Boyce, *Rubber Chem. Technol.* **72**, 633 (1999).

32. P.P. thanks the Fannie and John Hertz Foundation for support of his work through graduate fellowship. The authors thank Y. Elkasabi for help with FTIR spectroscopy and ellipsometry measurements; the staff of the Electron Microscopy Analysis Laboratory (Univ. of Michigan) and NSF (grant DMR-0320740); the Air Force Office of Scientific Research program on multifunctional materials (grant FA9550-05-1-043), and the U.S. Office of Naval Research (grant N00014-06-1-0473) for financial support.

Supporting Online Material
www.sciencemag.org/cgi/content/full/318/5847/80/DC1
Materials and Methods
Figs. S1 to S10
References

28 March 2007; accepted 4 September 2007
10.1126/science.1143176

Major Australian-Antarctic Plate Reorganization at Hawaiian-Emperor Bend Time

J. M. Whittaker,[1]* R. D. Müller,[1] G. Leitchenkov,[2] H. Stagg,[3] M. Sdrolias,[1] C. Gaina,[4] A. Goncharov[3]

A marked bend in the Hawaiian-Emperor seamount chain supposedly resulted from a recent major reorganization of the plate-mantle system there 50 million years ago. Although alternative mantle-driven and plate-shifting hypotheses have been proposed, no contemporaneous circum-Pacific plate events have been identified. We report reconstructions for Australia and Antarctica that reveal a major plate reorganization between 50 and 53 million years ago. Revised Pacific Ocean sea-floor reconstructions suggest that subduction of the Pacific-Izanagi spreading ridge and subsequent Marianas/Tonga-Kermadec subduction initiation may have been the ultimate causes of these events. Thus, these plate reconstructions solve long-standing continental fit problems and improve constraints on the motion between East and West Antarctica and global plate circuit closure.

A long-standing controversy in global tectonics concerns the ultimate driving forces that episodically cause major plate tectonic reorganizations. Proponents of "top-down" mechanisms [e.g., (*1*, *2*)] argue that plates themselves drive instabilities of the plate-mantle system, whereas others [e.g., (*3*)] have argued that major mantle overturns drive plate tectonic punctuations. The most prominent manifestation of this controversy is the Hawaiian-Emperor sea-